

Magnetolectric hysteresis of Bragg resonances in a multiferroic crystal based on YIG/HZOMaria A. Morozova * and Oleg V. Matveev *Laboratory “Magnetic Metamaterials”, Saratov State University, Saratov 410012, Russia*

Andrey M. Markeev, Anna G. Chernikova, and Alexander M. Mednikov

*Moscow Institute of Physics and Technology, Moscow Region, Dolgoprudny 141701, Russia*Sergey A. Gusev  and Igor Yu. Pashenkin*Institute for Physics of Microstructures, Russian Academy of Sciences, Nizhny Novgorod 603950, Russia*

Nikita S. Gusev

*Institute for Physics of Microstructures, Russian Academy of Sciences, Nizhny Novgorod 603950, Russia
and Lobachevsky State University of Nizhny Novgorod, Nizhny Novgorod 603022, Russia*

Dmitry V. Romanenko

Laboratory “Magnetic Metamaterials”, Saratov State University, Saratov 410012, Russia

Sergey A. Nikitov

*Laboratory “Magnetic Metamaterials”, Saratov State University, Saratov 410012, Russia
and Kotelnikov Institute of Radioengineering and Electronics, Russian Academy of Sciences, Moscow 125009, Russia*

(Received 31 May 2023; accepted 21 September 2023; published 6 November 2023)

This paper reports on the hysteresis and frequency tuning (electrical and magnetic) of the Bragg resonance in the spectrum of spin waves in a multiferroic structure based on YIG (100 nm thick) and HZO (10 nm thick) with a periodic modulation of parameters. The resonance can be tuned in a wide frequency range of 1–4 GHz by a magnetic field H and in a narrow frequency range of ~ 3 MHz by an electric field E . Electrical tuning was carried out due to a combination of the magnetostriction of the ferromagnetic layer and the piezoelectric effect in the ferroelectric due to mechanical coupling between the layers. The direction of the resonance shift caused by the electric field changed at the coercive field, and the alteration characteristic is of “butterfly” type.

DOI: [10.1103/PhysRevB.108.174407](https://doi.org/10.1103/PhysRevB.108.174407)**I. INTRODUCTION**

One of the alternative concepts to overcome the limitations imposed by standard complementary metal-oxide-semiconductor (CMOS) electronics lies in the field of magnonics, the basic principle of which is to use spin waves or magnons instead of electrons as information carriers [1]. One of the most promising materials in which spin-wave propagation is possible is yttrium iron garnet (YIG) ferromagnetic films, due to the low level of losses, the possibility of scaling up to several nanometers, low-energy consumption for the excitation of spin waves, and good integrability with semiconductor technologies [2–4].

However, the most promising way is the use of multiferroic materials, in which the properties of spin waves can be controlled not only with a magnetic field, but also with an electric field [5,6]. Artificial multiferroics include ferromagnetic and ferroelectric layers and exhibit both properties characteristic of each of the layers separately and new properties associated

with the interaction of the magnetic and electrical subsystems [7,8].

In such substances, a magnetolectric effect takes place, which manifests itself in a change in the magnetization of the sample under the action of an electric field (reverse effect). In layered structures, the effect arises as a result of a combination of the magnetostriction of the ferromagnetic layer and the piezoelectric effect in the ferroelectric layer due to the mechanical coupling between layers. It is shown that in the YIG/lead zirconate titanate (YIG/PZT) and YIG/lead magnesium niobate–lead titanate (YIG/PMN-PT) (10 μm /500 μm) structures, due to the noted effects, a ferromagnetic resonance frequency shift up to 4 MHz was observed when an electric field magnitude of up to 3 kV/cm was applied [9–11].

In turn, periodic structures based on multiferroic materials, multiferroic magnonic crystals (MMCs), due to the formation of Bragg resonances [band gaps (BGs), nontransmission bands] in the spectrum of spin waves, open up great opportunities for controlling waves, compared with homogeneous structures [12–15]. In particular, an electric field up to 3 kV/cm makes it possible to shift the BG of spin waves

*mamorozovama@yandex.ru

at 20 MHz in the YIG/PZT structure (10 $\mu\text{m}/500 \mu\text{m}$) [14]. In this case, the BG frequency shift depended linearly on the field, which indicates that the magnetic and piezoelectric layers operate in the linear sections of the characteristics.

However, at high electric field magnitudes, there is a hysteresis dependence of the polarization and deformation of ferroelectric and piezoelectric materials on the electric field [16,17]. It is shown that this feature, due to the magnetoelectric effect, leads to a hysteresis dependence of the ferromagnetic resonance frequency with an increase in the electric field magnitude up to 10 kV/cm in a homogeneous (nonperiodic) YIG/PZT structure (10 $\mu\text{m}/500 \mu\text{m}$) [16]. Note that the magnetoelectric effect has so far been observed only in thick multiferroic structures (several tens of μm), and the structures were composites (mechanical coupling was achieved using glue). In addition, the question of the effect of the ferroelectric and piezoelectric hysteresis on the characteristics of the spin-wave Bragg resonances in the magnetic subsystem of the MMC (periodic structure) remains open.

Currently, one of the promising ferroelectric materials are binary ferroelectric oxides based on hafnia [18–24], due to full integration into modern CMOS technologies, unlike ferroelectric and piezoelectric ceramics. Modern technologies make it possible to obtain hafnia films for several dopants with a thickness of 5–20 nm, which have the properties of ferroelectric and deformation hysteresis. In this case, the remnant polarization reached a value of 16 $\mu\text{C}/\text{cm}^2$, the maximum deformation was about 20 pm, and the number of rewrite cycles reaches 10^{10} [25–27]. These properties make hafnium oxide films a promising material for producing a nonvolatile memory such as ferroelectric random-access memory (FRAM), ferroelectric field-effect transistors (Fe-FETs), ferroelectric tunnel junctions (FTJs), ferroelectric based electrostatic doping (Fe-ED), resistive switching random-access memory (RRAM) [20–24].

This paper is dedicated to the study of the hysteresis properties of spin waves in a monolithic MMC based on YIG and hafnium-zirconium oxide (HZO) films, made on a nanometer scale. Main attention is paid to the electrical and magnetic tuning of the BG in the spectrum of spin waves. In this work, the MMC based on YIG and HZO layers was created; the experimental study of the hysteresis properties of the ferroelectric and ferromagnetic subsystems was carried out; the theoretical model was constructed to reveal the mechanism of the effect of hysteresis on the characteristics of the band gaps for spin waves.

II. EXPERIMENT

To create experimental layouts, we used a single-crystal film of yttrium iron garnet 111 (YIG, $\text{Y}_3\text{Fe}_5\text{O}_{12}$) with a thickness of $d = 100$ nm, saturation magnetization $M_0 = 140$ G, ferromagnetic resonance linewidth 0.5 Oe, grown by liquid-phase epitaxy on a gadolinium gallium garnet (GGG, $\text{Gd}_3\text{Ga}_5\text{O}_{12}$) 500 μm thick. High- k ($k > 20$) hafnium-zirconium oxide ($\text{Hf}_{0.5}\text{Zr}_{0.5}\text{O}_2$, HZO) in a ferroelectric orthorhombic phase was used as a ferroelectric layer. Titanium nitride (TiN) conductive layers were used to apply a voltage to polarize HZO. The TiN/HZO/TiN layered structure of thickness 20 nm/10 nm/20 nm was created on the surface of the YIG film. To create the TiN/HZO/TiN

structure, the atomic layer deposition (ALD) method was used, which is characterized by conformality and uniformity of coating surfaces of complex relief, as well as high reproducibility [26,28]. ALD of the TiN/HZO/TiN structure on the YIG surface was carried out on a Sunale R 150 setup (Picosun) equipped with a double-walled vertical chamber. Highly pure nitrogen was used to purge the chamber between reagent injections and as a carrier gas. A MidiGas nitrogen station (Parker) with an H04 compressor (Hydrovane) and a Pseudri Midas dryer (Domnick Hunter) was used as a nitrogen source. After deposition of the upper layer of TiN, a rapid thermal annealing (RTA) was carried out, which ensured the crystallization of HZO (at a temperature of 400 $^\circ\text{C}$ in an N_2 atmosphere), which made it possible to increase the value of the remanent polarization by 30%.

The experimental MMC structure was created based on the resulting five-layer film YIG/TiN/HZO/TiN. The setup consisted of a spin-wave waveguide with periodic thickness modulation, coplanar antennas for spin-wave excitation and reception in YIG, and contact pads to manipulate HZO polarization. Figure 1(a) shows a scheme of MMC. The waveguides were fabricated with photolithography technologies using auxiliary multilayer masks made of metal films and ion and plasma chemical etching methods. The waveguide was 40 μm long and 50 μm wide. Using explosive photolithography “lift-off” methods, a periodic system of grooves on the surface of the waveguides with a depth of 60 nm and a period of $L = 4 \mu\text{m}$ was created, as shown in Fig. 1(b). Thus, the TiN/HZO/TiN stripes were located on the YIG stacks. Figure 1(c) shows the results of atomic force microscopy measuring the surface profile of a periodic structure. To excite spin waves, coplanar antennas with a ground-signal-ground (GSG) configuration with a stripe width of 4 μm and the distance between the stripes of 2.5 μm with photolithography were created. Contact pads were formed on the surface of the bottom and top TiN layers (TiN-1 and TiN-2) to apply the control voltage and HZO polarization. A window to the TiN-2 layer was obtained by plasma etching. Figure 1(d) shows an image of the obtained structure in secondary electrons, obtained in a scanning electron microscope.

At the first step, electrophysical measurements of the ferroelectric properties of the YIG/TiN/HZO/TiN film were carried out. The electric field in the HZO layer was created by applying a constant voltage U to the TiN layers. The measurements were carried out by the positive up negative down (PUND) method [29], which makes it possible to separate the ferroelectric response from the linear induced polarization and possible parasitic effects. A sequence of PUND pulses with a pulse duration of 3 μs was applied to the sample, and the charge was measured in sections of constant voltage. Polarization was calculated as the difference between the integral over the electrical current from the first pulse and from subsequent pulses, thus eliminating the leakage current.

Figure 2(a) shows the resulting hysteresis dependence of the HZO polarization P on voltage. It can be seen that when a voltage of 3 V is applied (red curve), the remanent polarization (after 10^5 cycles) is $P_s = 8.5 \mu\text{C}/\text{cm}^2$, and the coercive voltage is $U_k = \pm 1.1$ V. When a voltage of 2.5 V (black curve) is applied, the remanent polarization (after 10^5 cycles) is 6.3 $\mu\text{C}/\text{cm}^2$. The green curve shows the polarization versus

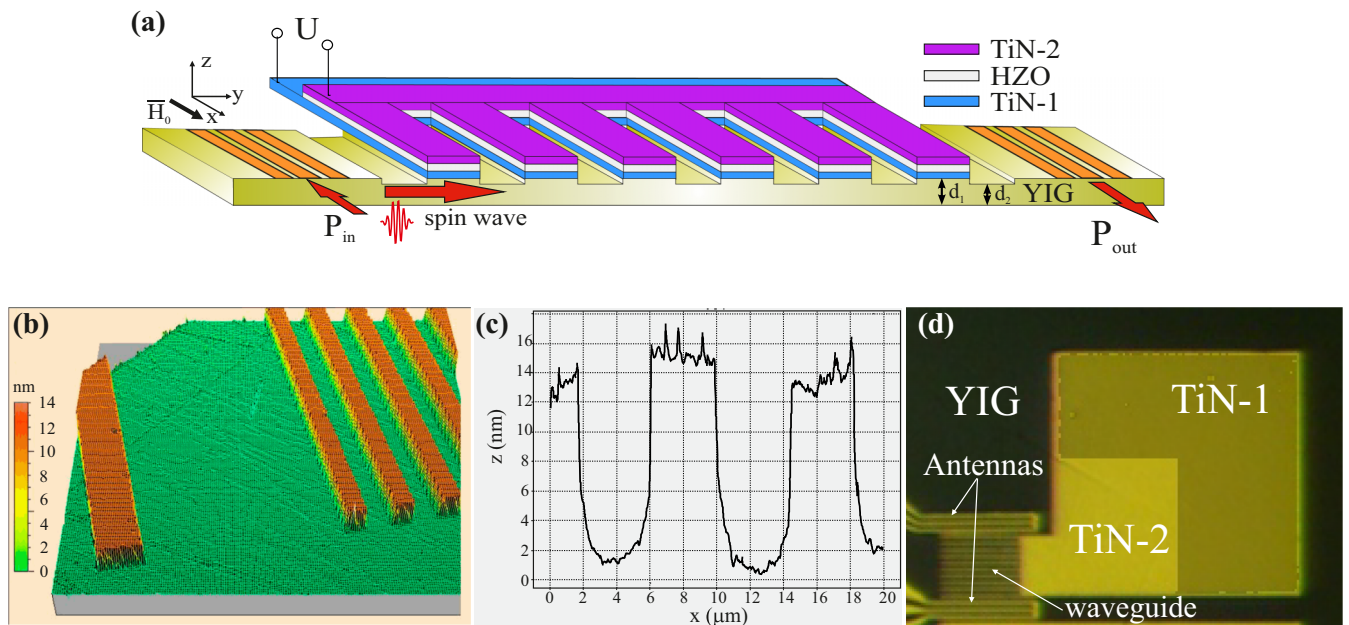


FIG. 1. (a) The scheme of the MMC structure. (b) Surface profile of the periodic structure of MMC obtained from an optical interferometer. (c) Surface profile of periodic structure of MMC obtained from an atomic force microscope. (d) Secondary electron detector image of the experimental layout from a scanning electron microscope.

voltage at 2.5 V on the pristine cycles. Thus, a two-level state of HZO (at switch voltages 2.5 and 3 V) is realized. The current-voltage characteristics also show ferroelectric switching peaks at U_k [Fig. 2(b)]. In addition, the wake-up effect is observed, which consists in an increase in the remanent polarization after 10^5 cycles by 20%–30% [see the insets to Figs. 2(b) and 2(a)].

At the second step, the propagation of spin waves in the magnetic subsystem was studied. An external magnetic field strength H_0 was applied parallel to the excitation

antennas in the direction of the z axis, so that surface spin waves can propagate along the y axis. We have used vector network analyzers Agilent Technologies ESA-E E4402B (9 kHz–3 GHz) and ESA-L E4408B (9 kHz–26.5 GHz), Planar C2220 (100 kHz–20 GHz) to study of spin-wave propagation, microwave probes Cascade SP-FPC-GSG-200-05 and FPC-W-GSG-200 for receiving/transmitting spin waves, and dc probes for applying voltage to a ferroelectric capacitor and microprobers. We have measured the amplitude-frequency characteristics of spin waves in a frequency range 1.5–6 GHz with input signal powers from –30 to 0 dBm. The measurements were carried out at room temperature.

Figures 3(a) and 3(b) show the amplitude-frequency characteristics and the corresponding dispersion characteristics obtained from the spin-wave phase-frequency measured data. From Fig. 3(a) it can be seen that at $U = 0$ (red curve) at a frequency f_{B0} a pronounced minimum is observed. At a frequency f_{B0} , there is also a jump in the dispersion characteristic [red curve in Fig. 3(b)], with the wave number coinciding with the wave number of the first Bragg resonance $k_B = \pi/L = 0.7853 \mu\text{m}^{-1}$. Consequently, the frequency f_{B0} is the center frequency of the first Bragg resonance [30–32]. The region of frequencies near f_{B0} is the band of nontransmission of spin waves—the first Bragg band gap [shown by the gray shading in Figs. 3(a) and 3(b)]. As the voltage increases to 3 V [orange curves in Figs. 3(a) and 3(b)], the BG shifts down in frequency by about 3 MHz and is observed at a frequency f_{BU} .

Figure 4 shows the transmission coefficient [$T = 10 \log(P_{\text{out}}/P_{\text{in}})$, where P_{out} is the power output, and P_{in} is the power input] versus frequency (amplitude-frequency characteristics) at various magnitudes of the external magnetic field. It can be seen that as the magnetic field magnitude increases from 120 to 880 Oe, the spin-wave excitation band shifts

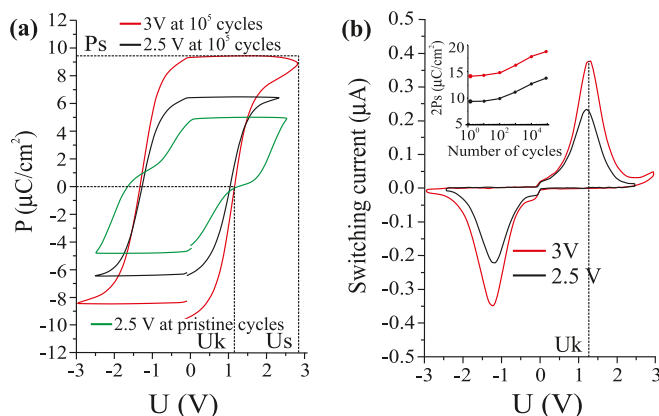


FIG. 2. (a) HZO polarization vs voltage measured after 10^5 cycles at a switching voltage of 3 V (red curves) and 2.5 V (black curves), on pristine cycles at a switching voltage of 2.5 V (green curve). (b) Current-voltage characteristics measured after 10^5 cycles at a switching voltage of 3 V (red curves) and 2.5 V (black curves). In the inset, the dependence of the remanent polarization on the number of cycles (wake-up curve) for a switching voltage of 2.5 V (black) and 3 V (red).

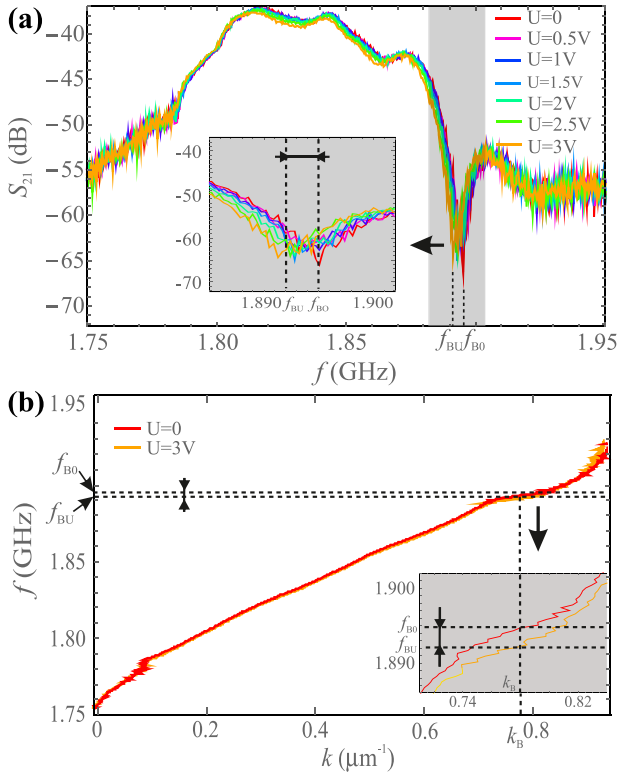


FIG. 3. (a) Amplitude-frequency and (b) dispersion characteristics of spin waves at $H_0 = 210$ Oe and various electrical voltages. The insets show fragments of the dependencies in the BG region.

upward in frequency, and the BG shift is about 3 GHz (see the bottom left inset).

Points of different colors in Fig. 5(a) show the dependencies of the shift of the BG center frequency $\Delta f = f_{B0} - f_{BU}$ on voltage at different magnitudes of the external magnetic field and the electric field polarity. We can distinguish two peculiar regions with different slope angles of the straight

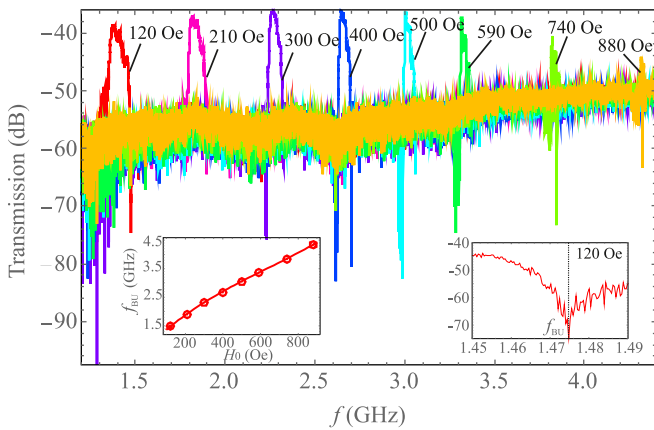


FIG. 4. Amplitude-frequency characteristics of spin waves at various strengths of the external magnetic field at $U = U_k = 1.1$ V. The bottom left inset shows the dependence of central frequency of the BGs on the external magnetic field. The bottom right inset shows the enlarged fragment of amplitude-frequency characteristics at $H_0 = 120$ Oe in the region of BG.

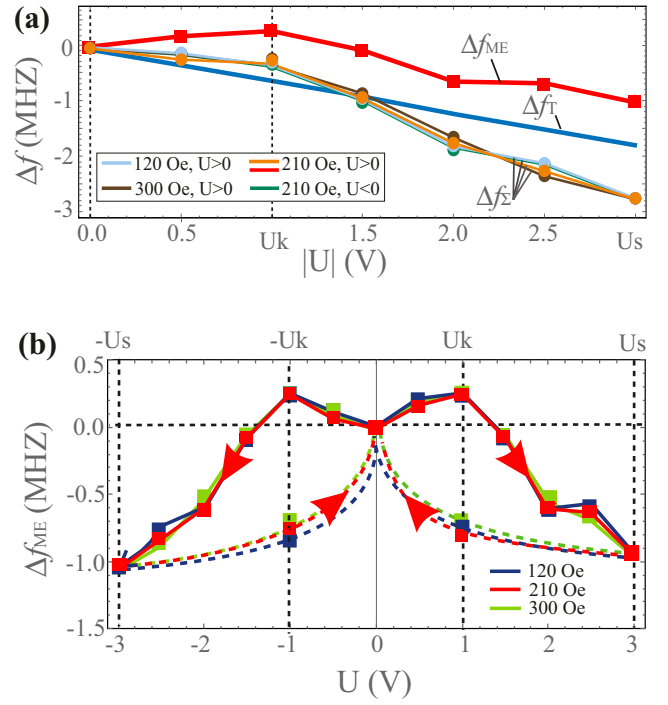


FIG. 5. (a) Dependencies of shift of the BG center frequency on the voltage due to both the magnetolectric effect and the heating at different H_0 and different polarities of the electric field (circles curves Δf_{Σ}), due only to the magnetolectric effect at $H_0 = 210$ Oe (squares, red curve Δf_{ME}), and due to only heating at different H_0 (blue curve). (b) Dependence of shift of the BG center frequency shift on the voltage at different H_0 ; the bypass direction is indicated by arrows.

lines on all dependencies: a region at $0 < U < U_k$ and at $U_k < U < U_s$. To explain this feature, it should be noted that when a voltage is applied to HZO, two main effects take place.

The first effect is the heating of the YIG and, as it is known, a change in the temperature of the YIG leads to a decrease in the saturation magnetization. A number of theoretical models have been proposed to describe the effect of heating a ferromagnetic layer on the saturation magnetization magnitude [33–35]. In the most general form, the temperature dependence of the YIG magnetization was obtained in Ref. [33], $M_0(T) = M_d(T) - M_a(T)$, where indices a and d correspond to the octahedral and tetrahedral YIG sublattices, respectively. The corresponding dependencies are described using the Brillouin functions $B_{S_a}(z_{ad})$ and $B_{S_d}(z_{da})$: $M_a(T) = M_a(0)B_{S_a}(z_{ad})$, $B_{S_a}(z_{ad}) = \frac{2S_a+1}{2S_a} \coth(\frac{2S_a+1}{2S_a} z_{ad}) - \frac{1}{2S_a} \coth(\frac{z_{ad}}{2S_a})$, $z_{ad} = g\mu_B S_a [N_{aa}M_a(T) + N_{ad}M_d(T)]/k'T$. The corresponding dependence for $M_d(T)$ is obtained by replacing the indices a by d and vice versa. $S_a = S_d = \frac{5}{2}$ are the spin quantum numbers of Fe^{3+} ions, $g = 2$ is the spectroscopic splitting factor, N_{aa} , N_{dd} , $N_{ad} = N_{da}$ are the molecular field coefficients in units of mol/cm^3 , μ_B is the Bohr magneton, and k' is the Boltzmann constant. At $T = 0$, the sublattice magnetization is expressed by the formulas $M_a(0) = 2g\mu_B S_a N$, $M_d(0) = 3g\mu_B S_d N$, where N is Avogadro's number. The temperature shift Δf_T was calculated according to the formula $\Delta f_T = f_T - f_{T=0}$, where f_T was calculated according to Eq. (4) taking into account

Eqs. (1)–(3), as described in Sec. III at $H_a = 0$, taking into account that M_0 depends on temperature. The temperature of the structure was measured with a thermal imager. The blue line in Fig. 5(a) shows the theoretical dependence of the center frequency shift of the BG on voltage due to YIG heating Δf_T .

The second effect is the magnetoelectric effect. The squares in Fig. 5(a) show the shift of the BG, due only to the magnetoelectric effect, and calculated as the difference between the total shift (orange curve) and the thermal shift (blue curve): $\Delta f_{ME} = \Delta f - \Delta f_T$.

Figure 5(b) shows the center frequency shift of the BG due to only the magnetoelectric effect (Δf_{ME}) during voltage cycling. With an increase in voltage in the range $0 < U < U_k$, the BG shifts up in frequency by 0.3 MHz; when the voltage changes in the range $U_k < U < U_s$, the BG shifts down in frequency by 1.3 MHz. The magnetoelectric coefficient in this case is $A = [\Delta f_{ME}(U = U_s) - \Delta f_{ME}(U = 0)]/U_s = 0.63$ MHz cm/MV. With the subsequent decrease in voltage to 0, the frequency of the BG increases to its original value. As a result, an alteration characteristic of the “butterfly” type was formed. The alteration characteristic qualitatively corresponds to the opposite dependence of the HZO layer deformation on the applied voltage [25].

III. THEORETICAL MODEL

To develop a theoretical model, we use the dispersion equation for spin waves, taking into account the exchange interaction in a ferromagnetic film without modulating parameters [36,37],

$$\omega_n^2 = [\omega_H + \omega_M \Lambda^2 k_n^2 + \omega_M (1 - \Phi)] \times (\omega_H + \omega_M \Lambda^2 k_n^2 + \omega_M \Phi \sin^2 \varphi_n), \quad (1)$$

where $\omega_H = \gamma H^0$, $\omega_M = \mu_0 \gamma M_0$, μ_0 is the vacuum permeability, γ is the gyromagnetic ratio, M_0 is the saturation magnetization, $H^0 = H_0 + H_a$ is the internal effective magnetic field, H_0 is the external magnetic field, H_a is the anisotropy field, $\Lambda^2 = \frac{2A_{ex}}{\mu_0 M_0^2}$, A_{ex} is the exchange constant, $\Phi = 1 - \frac{1 - e^{-k_n d}}{k_n d}$, d is the thickness, $k_n^2 = k^2 + k_{x,n}^2$, $\varphi_n = \arctan(k/k_{x,n})$, $k_{x,n} = n\pi/c$, c is the width, and $\omega_n = 2\pi f_n$, $n = 0, 1, 2, \dots$ is the mode number.

For a structure based on a ferromagnetic film loaded with a ferroelectric layer (FE), the reverse magnetoelectric effect takes place [6–8]. The nature of the phenomenon consists in the following. Any ferroelectric material is also piezoelectric, and a change in the sample polarization P , which occurs when a voltage U is applied to it, leads to its deformation. Deformation of the FE leads to the deformation of the ferromagnetic layer, which is mechanically coupled to the FE. In magnetic materials with magnetostriction, deformation leads to a change in the internal effective magnetic field, because of a change in the anisotropy field (Villari effect) [11,17].

The dependence of the anisotropy field on the sample deformation in a ferromagnetic medium with magnetostriction in isotropic case has the form [10,17,38,39]

$$H_a = \frac{3\lambda_s Y}{(1 + \mu)M_0} S(U), \quad (2)$$

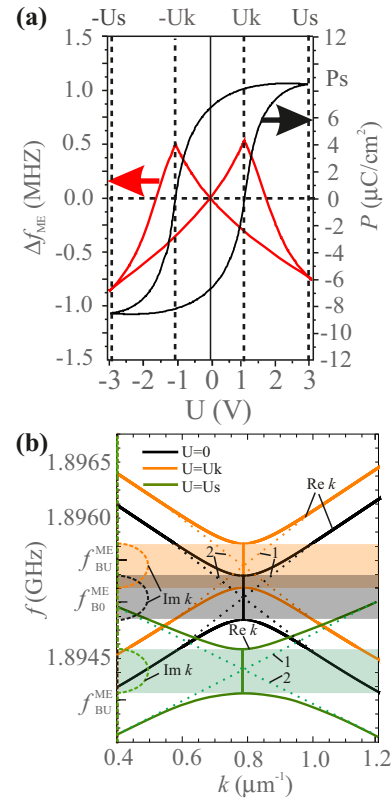


FIG. 6. (a) Dependence of ferroelectric polarization (black curve) and the center frequency of BG (red curve) on the shift of the voltage. (b) Dispersion characteristics of spin waves at $U = 0$ (black curve), $U = U_k = 1.1$ V (orange curve), $\text{Re}(k)$ (solid curves), $\text{Im}(k)$ (dashed curves). The characteristics of the direct and reflected waves in the absence of them are shown by point curves. Other parameters: $L = 4 \mu\text{m}$, $a = b = L/2$, $d_1 = 100$ nm, $d_2 = 90$ nm, $H_0 = 210$ Oe, $M_0 = 140$ G, $A_{ex} = 3.65 \times 10^{-12}$ J/m, $\lambda_{111} = -2.7 \times 10^{-5}$, $Y = 2 \times 10^{11}$ N/m², $n = 1$.

where λ_s is the magnetostriction constant, Y is the Young’s modulus, μ is the Poisson’s ratio, $S(U) = \Delta l(U)/l$ is the relative elongation (compression) of the structure, l is the size of the structure in the x direction, and $\Delta l(U)$ is the absolute strain when a stress U is applied.

The relative deformation of the HZO depends on the HZO polarization and has the properties of hysteresis of the “butterfly” type [25,27]. The analytical dependence of the polarization and deformation of FE materials can be written in the form of parametric equations [40]

$$S(\alpha) = |P(\alpha)|, \quad P(\alpha) = -\tilde{U}(\alpha) \cos \beta + \tilde{P}(\alpha) \sin \beta, \quad (3)$$

$$U(\alpha) = \tilde{U}(\alpha) \sin \beta + \tilde{P}(\alpha) \cos \beta,$$

where $\tilde{U}(\alpha) = \pm U_k \cos^3 \alpha \pm U_s \sin^3 \alpha$, $\tilde{P}(\alpha) = P_s \sin \alpha$, $\beta = \arctan \frac{(\epsilon-1)}{4\pi t}$, t is the FE thickness, and ϵ is the FE dielectric constant in the paraelectric phase.

The black curve in Fig. 6(a) shows the dependence of the polarization on U plotted according to Eq. (3) at $U_k = 1.1$ V, $U_s = 3$ V, $P_s = 8.5 \mu\text{C}/\text{cm}^2$, and $t = 10$ nm, with respect to the experimental data.

The investigated structure is a system of alternating sections of a ferromagnetic film of thickness d_1 , loaded with a FE

capacitor, and unloaded sections of the thickness d_2 , without a FE capacitor [see Fig. 1(a)]. The dispersion equation for spin waves in the structure under study can be obtained using the Hill equation [32] in the form

$$\cos(kL) = \cos(k_1a)\cos(k_2b) - \frac{1}{2}\left(\frac{k_1}{k_2} + \frac{k_2}{k_1}\right) \times \sin(k_1a)\sin(k_2b), \quad (4)$$

where L is the period; a, b are the section lengths; k_1 is the wave number of the spin wave in a film with thickness d_2 , where deformation of the FE leads to the appearance of an anisotropy field in this region ($H_a \neq 0$); and k_2 is the wave number of the spin wave in a film with thickness d_1 , which is not affected by deformation ($H_a = 0$).

Figure 6(b) shows the dispersion characteristics for spin waves in the investigated structure, calculated by Eq. (4), taking into account Eqs. (1)–(3) at different values of voltage U . It can be seen that the presence of a spatial period leads to the appearance of nontransmission bands in the spectrum of spin waves—band gaps (shown by color shading, central frequencies f_{B0}^{ME}, f_{BU}^{ME}), in which $\text{Im}(k) \neq 0$. BGs are formed at the frequencies of the phase matching of the direct waves (point lines 1) and waves, reflected from periodic inhomogeneities (point lines 2). The red curve in Fig. 6(a) shows the dependence of the shift of the center frequency of the BG $\Delta f_{ME}(U) = f_{B0}^{ME} - f_{BU}^{ME}(U)$ on the applied voltage U . It can be seen that the dependence has the “butterfly” form, as was early observed in the experiment [Fig. 5(b)]. The direction of the central frequency shift of the BG changes at the coercive voltage $\pm U_k$. The form of the alteration characteristic is preserved when the magnitude of the magnetic field changes.

Thus, the theoretical model makes it possible to explain the physical mechanism of Bragg resonance hysteresis in YIG/HZO obtained in the experiment. It is established that the resonance is caused by the presence of modulation of the thickness and anisotropy field in YIG in the direction of propagation of the spin waves. Anisotropy field hysteresis in YIG comes into existence of HZO polarization hysteresis due to the combination of the magnetostriction of YIG and the piezoelectric effect in HZO.

IV. CONCLUSION

Thus, we have demonstrated the hysteresis and frequency tuning (electrical and magnetic) of the Bragg resonance in the spectrum of spin waves in an MMC based on YIG/TiN/HZO/TiN (100 nm/20 nm/10 nm/20 nm) with periodic modulation of the parameters.

The originality of the structure lies, first, in the technology of creation using the liquid-phase epitaxy of YIG film and the atomic layer deposition of TiN and HZO films, which makes it

possible to effectively combine the layers and allows to keep the ferromagnetic and ferroelectric properties of each layer. Second, such a structure is a monolithic multiferroic structure with layer thicknesses on the order of tens of nanometers, which demonstrates the interaction of the magnetic and ferroelectric subsystems. Third, the developed technology for creating grooves on the surface makes such a structure a Bragg reflecting grating.

In particular, it is shown that the HZO layer in the composition of the MMC demonstrates the hysteresis property (saturation voltage up to 3 V, remanent polarization up to $9.2 \mu\text{C}/\text{cm}^2$), a two-level state, and the wake-up effect. In the YIG layer, the propagation of spin waves at frequencies of 1–4 GHz with a change in the magnetic field of 120–800 Oe was discovered. A Bragg band gap is observed in the spin-wave excitation band. The position of the band gap depends on the voltage (HZO polarization); when the voltage changes to 3 V, the frequency tuning is up to 1.3 MHz; the direction of the BG shift on the electric field changed at a coercive voltage of 1.1 V. The alteration characteristic is of the “butterfly” type.

The theoretical model is developed and it is shown that the main mechanism for the formation of a band gap is the interaction of direct and reflected spin waves from periodic inhomogeneities. When a voltage is applied to the ferroelectric layer and its polarization changes, a magnetoelectric effect takes place, which affects the mechanism of interaction between the direct and reflected waves. As a result, the position of the band gap in the spectrum of spin waves is determined by the remanent polarization of the ferroelectric layer and also has the property of hysteresis.

The practical importance of the result lies in the fact that the hysteresis dependence of the Bragg resonance of spin waves on the ferroelectric polarization, which was revealed in a nanoscale monolithic multiferroic structure, makes it possible to use such a structure as a memory cell. To write data, an effect of ferroelectric hysteresis in HZO is used; contrary, to read data, a spin wave in YIG at the Bragg resonance frequency is used. This memory cell will allow combining the advantages of ferroelectricity and magnonics in one structure and can be integrated into modern CMOS electronics.

ACKNOWLEDGMENTS

Experimental high-frequency measurements and theory investigation were supported by the Russian Science Foundation (Grant No. 23-79-30027 [41]). ALD of TiN/HZO/TiN structures and polarization versus voltage measurements were supported by the Russian Science Foundation (Grant No. 23-19-00227). The lithography was done using equipment of the Center of “Physics and Technology of Micro- and Nanostructures” at the Institute for Physics of Microstructures, Russian Academy of Sciences.

[1] A. Barman, G. Gubbiotti, S. Ladak, A. O. Adeyeye, M. Krawczyk, J. Gräfe, C. Adelman, S. Cotozana, A. Naeemi, V. I. Vasychka, B. Hillebrands, S. A. Nikitov, H. Yu, D. Grundler, A. V. Sadovnikov, A. A. Grachev, S. E. Sheshukova, J.-Y. Duquesne, M. Marangolo, G. Csaba *et al.*, The 2021 magnonics roadmap, *J. Phys.: Condens. Matter* **33**, 413001 (2021).

[2] Q. Wang, M. Kewenig, M. Schneider, R. Verba, F. Kohl, B. Heinz, M. Geilen, M. Mohseni, B. Lägél, F. Ciubotaru, C. Adelman, C. Dubs, S. D. Cotozana, O. V. Dobrovolskiy, T. Brächer, P. Pirro, and A. V. Chumak, A magnonic directional coupler for integrated magnonic half-adders, *Nat. Electron.* **3**, 765 (2020).

- [3] H. Qin, R. B. Holländer, L. Flajšman, F. Hermann, R. Dreyer, G. Woltersdorf, and S. van Dijken, Nanoscale magnonic Fabry-Pérot resonator for low-loss spin-wave manipulation, *Nat. Commun.* **12**, 2293 (2021).
- [4] B. Heinz, T. Brächer, M. Schneider, Q. Wang, B. Lägel, A. M. Friedel, D. Breitbach, S. Steinert, T. Meyer, M. Kewenig, C. Dubs, P. Pirro, and A. V. Chumak, Propagation of spin-wave packets in individual nanosized yttrium iron garnet magnonic conduits, *Nano Lett.* **20**, 4220 (2020).
- [5] V. Garcia, M. Bibes, and A. Barthélémy, Artificial multiferroic heterostructures for an electric control of magnetic properties, *C. R. Phys.* **16**, 168 (2015).
- [6] A. P. Pyatakov and A. K. Zvezdin, Magnetolectric and multiferroic media, *Phys. Usp.* **55**, 557 (2012).
- [7] N. X. Sun and G. Srinivasan, Voltage control of magnetism in multiferroic heterostructures and devices, *SPIN* **02**, 1240004 (2012).
- [8] C.-W. Nan, M. I. Bichurin, S. Dong, D. Viehland, and G. Srinivasan, Multiferroic magnetolectric composites: Historical perspective, status, and future directions, *J. Appl. Phys.* **103**, 031101 (2008).
- [9] A. B. Ustinov, Y. K. Fetisov, and G. Srinivasan, Planar ferrite-piezoelectric composite microwave resonator with electric and magnetic frequency tuning, *Tech. Phys. Lett.* **34**, 593 (2008).
- [10] Y. K. Fetisov and G. Srinivasan, Electric field tuning characteristics of a ferrite-piezoelectric microwave resonator, *Appl. Phys. Lett.* **88**, 143503 (2006).
- [11] G. Srinivasan and Y. K. Fetisov, Ferrite-piezoelectric layered structures: Microwave magnetolectric effects and electric field tunable devices, *Ferroelectrics* **342**, 65 (2006).
- [12] A. A. Nikitin, A. A. Nikitin, A. V. Kondrashov, A. B. Ustinov, B. A. Kalinikos, and E. Lähderanta, Theory of dual-tunable thin-film multiferroic magnonic crystal, *J. Appl. Phys.* **122**, 153903 (2017).
- [13] I. A. Ustinova, A. A. Nikitin, and A. B. Ustinov, Dynamic magnonic crystal based on a layered ferrite-ferroelectric structure, *Tech. Phys.* **61**, 473 (2016).
- [14] A. A. Grachev, O. V. Matveev, M. Mruczkiewicz, M. A. Morozova, E. N. Beginin, S. E. Sheshukova, and A. V. Sadovnikov, Strain-mediated tunability of spin-wave spectra in the adjacent magnonic crystal stripes with piezoelectric layer, *Appl. Phys. Lett.* **118**, 262405 (2021).
- [15] A. V. Sadovnikov, A. A. Grachev, S. E. Sheshukova, Y. P. Sharaevskii, A. A. Serdobintsev, D. M. Mitin, and S. A. Nikitov, Magnon straintronics: Reconfigurable spin-wave routing in strain-controlled bilateral magnetic stripes, *Phys. Rev. Lett.* **120**, 257203 (2018).
- [16] Y. K. Fetisov and G. Srinivasan, Nonlinear electric field tuning characteristics of yttrium iron garnet-lead zirconate titanate microwave resonators, *Appl. Phys. Lett.* **93**, 033508 (2008).
- [17] G. Srinivasan, I. V. Zavislyak, and A. S. Tatarenko, Millimeter-wave magnetolectric effects in bilayers of barium hexaferrite and lead zirconate titanate, *Appl. Phys. Lett.* **89**, 152508 (2006).
- [18] M. H. Park, Y. H. Lee, T. Mikolajick, U. Schroeder, and C. S. Hwang, Review and perspective on ferroelectric HfO₂-based thin films for memory applications, *MRS Commun.* **8**, 795 (2018).
- [19] *Ferroelectricity in Doped Hafnium Oxide: Materials, Properties and Devices*, edited by U. Schroeder, C. S. Hwang, and H. Funakubo (Elsevier, Amsterdam, 2019).
- [20] I. Shvetsov-Shilovskiy, A. Boruzdina, A. Ulanova, O. Orlov, Y. Matveev, and D. Negrov, FRAM test memory cells radiation hardness research, in *2017 IEEE 30th International Conference on Microelectronics (MIEL)* (IEEE, New York, 2017).
- [21] T. Ali, P. Polakowski, S. Riedel, T. Buttner, T. Kampfe, M. Rudolph, B. Patzold, K. Seidel, D. Lohr, R. Hoffmann, M. Czernohorsky, K. Kuhnelt, P. Steinke, J. Calvo, K. Zimmermann, and J. Muller, High endurance ferroelectric hafnium oxide-based FeFET memory without retention penalty, *IEEE Trans. Electron Devices* **65**, 3769 (2018).
- [22] S.-H. Tsai, Z. Fang, X. Wang, U. Chand, C.-K. Chen, S. Hooda, M. Sivan, J. Pan, E. Zamburg, and A. V.-Y. Thean, Stress-memorized HZO for high-performance ferroelectric field-effect memristor, *ACS Appl. Electron. Mater.* **4**, 1642 (2022).
- [23] D. Yao, L. Li, Y. Zhang, Y. Peng, J. Zhou, G. Han, Y. Liu, and Y. Hao, Energy-efficient non-volatile ferroelectric based electrostatic doping multilevel optical readout memory, *Opt. Express* **30**, 13572 (2022).
- [24] V. Mikheev, A. Chouprik, Y. Lebedinskii, S. Zarubin, A. M. Markeev, A. V. Zenkevich, and D. Negrov, Memristor with a ferroelectric HfO₂ layer: In which case it is a ferroelectric tunnel junction, *Nanotechnology* **31**, 215205 (2020).
- [25] J. Müller, T. S. Böske, D. Bräuhäus, U. Schröder, U. Böttger, J. Sundqvist, P. Kücher, T. Mikolajick, and L. Frey, Ferroelectric Zr_{0.5}Hf_{0.5}O₂ thin films for nonvolatile memory applications, *Appl. Phys. Lett.* **99**, 112901 (2011).
- [26] S. Zarubin, E. Suvorova, M. Spiridonov, D. Negrov, A. Chernikova, A. Markeev, and A. Zenkevich, Fully ALD-grown TiN/Hf_{0.5}Zr_{0.5}O₂/TiN stacks: Ferroelectric and structural properties, *Appl. Phys. Lett.* **109**, 192903 (2016).
- [27] S. Starschich, T. Schenk, U. Schroeder, and U. Boettger, Ferroelectric and piezoelectric properties of Hf_{1-x}Zr_xO₂ and pure ZrO₂ films, *Appl. Phys. Lett.* **110**, 182905 (2017).
- [28] A. G. Chernikova, M. G. Kozodaev, D. V. Negrov, E. V. Korostylev, M. H. Park, U. Schroeder, C. S. Hwang, and A. M. Markeev, Improved ferroelectric switching endurance of La-doped Hf_{0.5}Zr_{0.5}O₂ thin films, *ACS Appl. Mater. Interfaces* **10**, 2701 (2018).
- [29] *Ferroelectric Random Access Memories: Fundamentals and Applications*, edited by H. Ishiwara, M. Okuyama, and Y. Arimoto, Topics in Applied Physics Vol. 93 (Springer, Berlin, 2004).
- [30] S. Nikitov, P. Tailhades, and C. Tsai, Spin waves in periodic magnetic structures—magnonic crystals, *J. Magn. Magn. Mater.* **236**, 320 (2001).
- [31] M. Krawczyk and D. Grundler, Review and prospects of magnonic crystals and devices with reprogrammable band structure, *J. Phys.: Condens. Matter* **26**, 123202 (2014).
- [32] L. Brillouin and M. Parodi, *Wave Propagation in Periodic Structures* (Dover, New York, 1953).
- [33] P. Hansen, P. Röschmann, and W. Tolksdorf, Saturation magnetization of gallium-substituted yttrium iron garnet, *J. Appl. Phys.* **45**, 2728 (1974).
- [34] H. Algra and P. Hansen, Temperature dependence of the saturation magnetization of ion-implanted YIG films, *Appl. Phys. A* **29**, 83 (1982).
- [35] T. Langner, D. A. Bozhko, S. A. Bunyaev, G. N. Kakazei, A. V. Chumak, A. A. Serga, B. Hillebrands, and V. I. Vasyuchka,

- Spin-wave propagation through a magnonic crystal in a thermal gradient, *J. Phys. D: Appl. Phys.* **51**, 344002 (2018).
- [36] B. A. Kalinikos and A. N. Slavin, Theory of dipole-exchange spin wave spectrum for ferromagnetic films with mixed exchange boundary conditions, *J. Phys. C: Solid State Phys.* **19**, 7013 (1986).
- [37] H. Qin, S. J. Hämäläinen, K. Arjas, J. Witteveen, and S. van Dijken, Propagating spin waves in nanometer-thick yttrium iron garnet films: Dependence on wave vector, magnetic field strength, and angle, *Phys. Rev. B* **98**, 224422 (2018).
- [38] N. Sun, S. Priya, and G. Srinivasan, *Composite Magneto-electrics: Materials, Structures, and Applications* (Elsevier, Amsterdam, 2015).
- [39] S. Krupicka, *Physik der Ferrite und der verwandten magnetischen Oxide* (Springer, Berlin, 1973).
- [40] R. V. Lapshin, Analytical model for the approximation of hysteresis loop and its application to the scanning tunneling microscope, *Rev. Sci. Instrum.* **66**, 4718 (1995).
- [41] <https://rscf.ru/project/23-79-30027/>.